Microchimica Acta (2020) 187:281
https://doi.org/10.1007/s00604-020-04254-2

ORIGINAL PAPER

A chemiluminescence assay for determination of lysozyme based on the use of magnetic alginate-aptamer composition and hemin@HKUST-1

Yanna Lin[1] · Yuanling Sun[1] · Yuxue Dai[1] · Xiaodong Zhu[1] · Hao Liu[1] · Rui Han[1] · Dandan Gao[1] · Chuannan Luo[1] · Xueying Wang[1]

Received: 2 October 2019 / Accepted: 31 March 2020

Abstract

Lysozyme aptamer-functionalized magnetic alginate hydrogel was prepared for separation and enrichment of lysozyme. Luminol-labeled aptamer was used as a signal tag, and the signal tag was adsorbed on magnetic carboxylated carbon nanotubes based on the π-interaction. When lysozyme was added, the aptamer specifically binds to the lysozyme, causing the signal tag to detach from the magnetic carboxylated carbon nanotubes. When the aptamer/lysozyme complex bound to the complementary single strand of aptamer on the hemin@HKUST-1, lysozyme was released. The released lysozyme can be recombined with the signal tag adsorbed on the magnetic carboxylated carbon nanotube, allowing more signal tag to be dispersed into the solution. Determination of lysozyme was achieved by releasing the luminol-labeled aptamer to generate a chemiluminescence signal at a wavelength of 425 nm. It was proved by experiments that the synthesized hemin@HKUST-1 had a strong catalytic effect on the luminol-NaOH-H_2O_2 system. The chemiluminescence signal was increased nearly 100 times. The complementary pairing allowed the luminol to be immobilized on the surface of hemin@HKUST-1. The generation and consumption of short-lived reactive oxygen species were concentrated on the surface of the MOFs, which improves the chemiluminescence efficiency. The introduction of hemin@HKUST-1 and DNA solved the defects of chemiluminescence analysis. The chemiluminescence assay was able to detect lysozyme with linear range of 1.05×10^{-6} U·mg^{-1} (6.00×10^{-13} mol·L^{-1})–1.25×10^{-2} U·mg^{-1} (7.14×10^{-9} mol·L^{-1}); the detection limit was 3.50×10^{-7} U·mg^{-1} (2.00×10^{-13} mol·L^{-1}) ($R^2 = 0.99$). The recovery of lysozyme in spiked saliva samples was 97.4–102.8%.

Keywords Carbon nanotube · Target recycling · Signal amplification · Protein · Enzyme · Catalytic effect · MOFs · Biosensor · DNA · Signal tag

Introduction

Magnetic nanomaterials are favored because of their characteristics of both nanomaterials and magnetic materials. The magnetic nanomaterials have been widely used in the fields of separation [1], adsorption [2, 3], drug targeted delivery [4, 5], and water treatment [6]. The chemical experiment process should follow the "5R" principles of green chemistry, namely reduction, reuse, recycling, regeneration, and rejection. Among them, "rejection" means refusing toxic and harmful products, which is the most fundamental approach to prevent pollution.

Sodium alginate is safe and nonpolluting. It is able to physically crosslink with Ca^{2+} to form a gel, and the magnetic calcium alginate hydrogel had been used to remove the heavy metal from aqueous solutions [7]. Alginate has excellent

Electronic supplementary material The online version of this article (https://doi.org/10.1007/s00604-020-04254-2) contains supplementary material, which is available to authorized users.

✉ Chuannan Luo
chm_yfl518@163.com

✉ Xueying Wang
chm_wangxy@ujn.edu.cn

[1] Key Laboratory of Interfacial Reaction & Sensing Analysis in Universities of Shandong, School of Chemistry and Chemical Engineering, University of Jinan, Jinan 250022, People's Republic of China

Published online: 20 April 2020

biocompatibility and contains a large amount of carboxyl groups, providing a platform for the bonding of biomolecules [8]. Therefore, the nanomaterials based on magnetic alginate are potential candidates for biomolecules separation.

Chemiluminescence (CL) is one of the commonly used analytical methods. However, the sensitivity of simple CL analysis cannot satisfy the actual detection. Signal amplification strategy is one of the effective methods to improve the sensitivity of analytical methods. Based on it, biological enzymes or catalytically active nanomaterials were introduced into CL analysis to improve the sensitivity of the sensor [9, 10]. However, biology enzymes are low in stability [11] and easily to inactivate or form dimer [12] in aqueous solution. The phenomenon limit the use of enzymes in biosensors. Biological enzyme immobilization technology is one of the effective methods to overcome the shortcomings of free enzymes [13].

As one of the emerging porous materials, metal-organic framework (MOF) materials have been favored by researchers. The excellent performance makes it possible for its application in biological analysis. Liu et al. [14] immobilized glucose oxidase (or uricase) and horseradish peroxidase on hierarchically porous MOFs and constructed two colorimetric biosensors for glucose and uric acid. The results indicated that the enzyme-MOFs composites exhibits a rapid catalytic rate. Alizadeh et al. [15] prepared Ni-hemin MOFs mimetic enzyme by assembling Ni^{2+} and hemin. They proved that the artificial enzyme possesses surprising peroxidase activity. Based on this, they constructed a colorimetric sensor for detection of tumor cell and obtained a satisfactory result. In addition, the group of Chi [16] synthesized a novel MOFs by encapsulating hemin into the HKUST-1 (hemin@HKUST-1). They demonstrated that the hemin@HKUST-1 enhances the CL intensity of the luminol-H_2O_2 system by 100 times. They used hemin@HKUST-1 to construct a CL sensor for detecting glucose and H_2O_2 with wide response range and low detection limit. In summary, catalyst functionalized MOFs have potential in biological applications. However, the application of MOFs is still in preliminary stage and needs to be further explored.

Lysozyme plays an important role in human non-specific immunity. It was found that decreased levels of lysozyme are associated with neonatal bronchopulmonary dysplasia [17]. In addition, the level of lysozyme in serum is also associated with certain cancers and nodular diseases [18]. Thus, it is of great significance to develop a selective, sensitive, and accurate method for detecting lysozyme. The detection methods mainly include electrochemistry [19–21], chemiluminescence [22], fluorescence [23], and colorimetry [24].

Herein, a CL assay for detecting lysozyme was developed. Using magnetic alginate-aptamer composition (M-Alg-Apt) as the separation material, aptamer-luminol complex (Apt-luminol) as signal tag, and HKUST-1 encapsulated hemin (hemin@HKUST-1) as the catalyst, 100 times amplification of the CL signal was achieved. Finally, the method has been successfully used for the detection of lysozyme in saliva, indicating that the CL method has potential in practical application.

Experimental section

Reagents and materials

Na_2CO_3, $CaCl_2$, and ethylenediaminetetraacetic acid (EDTA) were purchased from Sinopharm Chemical Reagent Co., Ltd. (https://www.sinoreagent.com). $FeCl_3$ and $FeCl_2$ were obtained from Damao Chemical Reagent Factory (Tianjin, China, http://www.dmreagent.com/). Carbon nanotubes was ordered from Deke Island Gold Technology Co., Ltd. (http://www.nanoinglobal.com/). $Cu(NO_3)_2{\cdot}3H_2O$ was obtained from Tianjin Baishi Chemical Co., Ltd. (Tianjin, China, http://www.tjbschem.com/). Trimesic acid (H_3BTC, 98%) and Fe_3O_4 were purchased from Aladdin Biochemical Technology Co., Ltd. (Shanghai, China, https://www.aladdin-e.com/). N, N-dimethylformamide (DMF) and acetic acid (98%) were offered by Fuyu Fine Chemical Co., Ltd. (https://fuyuhuagong.cn.china.cn/). 1-(3-dimethylaminopropyl)-3-ethylcarbodiimide hydrochloride (EDC, 95%) was obtained from Saan Chemical Technology Co., Ltd. (Shanghai, China, https://www.energy-chemical.com/). N-hydroxysuccinimide (NHS) was obtained from Shanghai Civi Chemical Technology Co., Ltd. (Shanghai, China, http://www.civi-chem.com/). NH_2-aptamer (Apt), cDNA, and hemin were ordered from Sangon Biotech (Shanghai, China, https://www.sangon.com/) Co., Ltd. The oligonucleotides sequences are as follows:

NH_2-aptamer: 5′-NH_2-ATC TAC GAA TTC ATC AGG GCT AAA GAG TGC AGA GTT ACT TAG-3′
Complementary single strand of aptamer (cDNA): 5′-NH_2-CTA AGT AAC TCT GCA CTC TTT AGC CCT GAT GAA TTC GTA GAT-3′
Buffer used in experiments was the phosphate buffer (pH = 7.4).

Apparatus

The morphology and diameter of Fe_3O_4@$CaCO_3$, magnetic alginate (M-Alg), hemin@HKUST-1, and magnetic carboxylated carbon nanotubes (MCNTs) were characterized by JEM-2100 scanning electron microscope (SEM, Tokyo, Japan, https://www.jeol.co.jp/en/) and JEOL 1400 transmission electron microscopy (TEM, Tokyo, Japan, https://www.jeol.co.jp/en/). The crystal structure and lattice parameters of M-Alg, hemin@

HKUST-1, and MCNTs were obtained from a D8 focus diffractometer (D8 Advance, Bruker, Germany, https://www.bruker.com). VERTEX70 Fourier transform infrared spectrometer (FTIR, Bruker, Germany, https://www.bruker.com/cn/) was used to explore the functional group composition in M-Alg, hemin@HKUST-1, and MCNTs. A fully automatic surface area and pore size analyzer (TristarII, Shanghai, China, http://www.shjinghong.com/) was used to explore the adsorption properties of hemin@HKUST-1. All CL experiments were performed by the MPI-F flow injection chemiluminescence analyzer from Xi'an Remex Analysis Instrument Co., Ltd. (Xi'an, China, http://www.chinaremex.com/).

Synthesis of M-Alg-apt

Fe_3O_4@$CaCO_3$ was prepared according to the reported reference [25]. The detail was described in the Electronic Supplementary Material (section S1). A total of 0.2 g of Fe_3O_4@$CaCO_3$ was dispersed in 50 mL of water to obtain the solution 1; 0.3 g of sodium alginate and 0.1 g of gluconolactone were dissolved in 50 mL of water to obtain the solution 2. The solution 1 and solution 2 were mixed under stirring. After stirring at room temperature for 1 h, M-Alg was obtained. A total of 0.8 g of EDC and 0.7 g of NHS were added to the M-Alg. After activation for 30 min, an appropriate amount of lysozyme aptamer was added, and the mixture was stirred for 2 h to obtain the M-Alg-Apt.

Synthesis of hemin@HKUST-1-cDNA

The synthesis of hemin@HKUST-1 was performed according to the previous method [26]. The detailed preparation processes of hemin@HKUST-1 and hemin@HKUST-1-cDNA are shown in Electronic Supplementary Material (S2).

Synthesis of MCNTs/Apt-luminol

The synthesis of MCNTs/Apt-luminol is shown in Electronic Supplementary Material (S3).

Determination of lysozyme

(1) Measurement of CL intensity of the blank control group. The lysozyme sample was not added to the MCNTs/Apt-luminol solution. The CL intensity of the supernatant was measured by the instrument in the presence of an external magnetic field, $I_0 = 0$.
(2) After lysozyme sample was added, the CL intensity of the system supernatant was measured. The lysozyme sample was added to the MCNTs/Apt-luminol solution, and the CL intensity value I_1 of the supernatant was measured by the instrument in the presence of an external magnetic field. The actual CL intensity value $I = I_1$.

Results and discussion

Working principle of the assay

As shown in scheme 1, M-Alg-Apt was synthesized for the separation and enrichment of lysozyme. Apt-luminol acted as signal tag and was adsorbed on MCNTs based on the π-interaction. When lysozyme isolated from complex sample was added, Apt-luminol was detached from MCNTs due to the formation of the Apt-luminol/lysozyme conjugates. The aptamer was fully complementary to the cDNA on the hemin@HKUST-1/cDNA, allowing lysozyme to be released. Thus, the released lysozyme bound to the remaining Apt-luminol on the MCNTs, releasing more signal tags. It was worth noting that Apt-luminol was immobilized on the surface of hemin@HKUST-1/cDNA so that the generated reactive oxygen species can react with luminol in time. The diffusion distance between reactive oxygen species and luminol was shortened, and the CL efficiency was improved. Finally, sensitive detection of lysozyme was achieved.

Characterizations of M-Alg and MCNTs

The synthesized M-Alg and MCNTs were characterized by SEM, XRD, and FTIR. The results of characterization indicate that the M-Alg and MCNTs were synthesized successfully. The detailed description is shown in Electronic Supplementary Material (Fig. S1 and Fig. S2).

Characterization of hemin@HKUST-1

The nature of hemin@HKUST-1 was explored. Figure 1a shows that the hemin@HKUST-1 had a significant cubic structure with a size of approximately 500 nm. The BET characterization indicates that the hemin@HKUST-1 possessed the type-I adsorption isotherm characteristic of the microporous material. The measured BET surface area was 637.1452 $m^2 \cdot g^{-1}$, which laid a foundation for its catalysis. In the FTIR (Fig. 1c), the absorption peak at 3664 cm^{-1} was produced by the stretching vibration of O-H. The absorption peak at 2941 cm^{-1} was stretching vibration peak of the C-H on pyrrole ring. The peak at 1500 cm^{-1} was caused by the vibration of benzene ring skeleton. Peaks at 1666 cm^{-1} and 1423 cm^{-1} were the characteristic peak of Cu-O-CO. The absorption peak at 1345 cm^{-1} was generated by C=N stretching vibration. The peak at 1010 cm^{-1} was the characteristic peak of the metalloporphyrin. The absorption peak at 599 cm^{-1} was the stretching vibration peak of C-H on the benzene ring. In the XRD pattern (Fig. 1d), $2\theta = 11.6°$, 13.4°, 17.4°, 19°, 20.2°, 25.9°, 29.3°, 35.2°, and 39.1° correspond to crystal surface (222), (400), (333), (440), (600), (731), (555), (773), and (131), respectively, indicating that

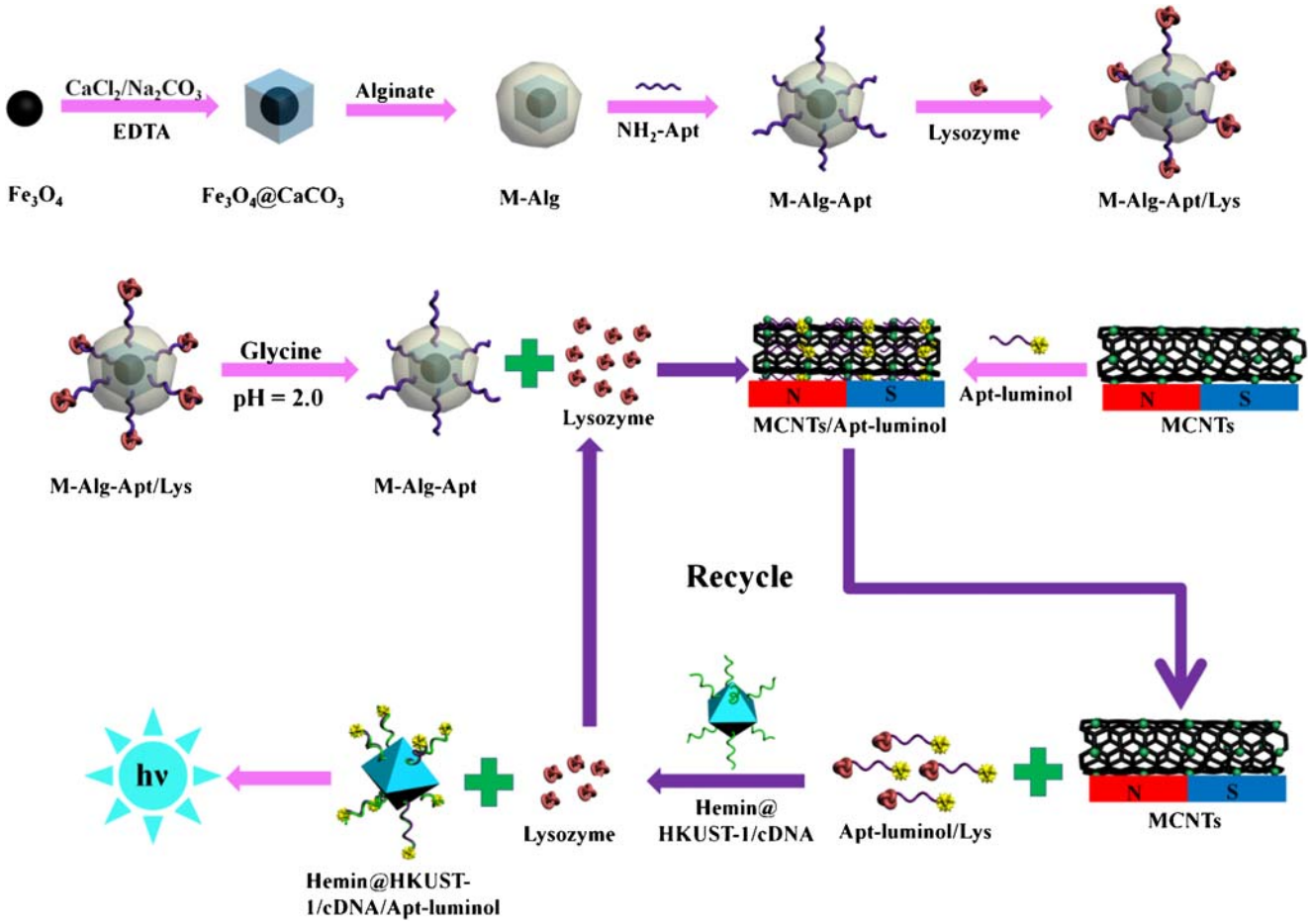

Scheme 1 Schematic illustration of the CL assay based on the amplification of hemin@HKUST-1

the incorporation of hemin has no effect on the crystal structure of HKUST-1.

Adsorption property of MCNTs

The Apt-luminol conjugate was added to the MCNTs dispersion. After incubation overnight, Apt-luminol/MCNTs were separated in an external magnetic field to obtain the supernatant. The absorbance (A) of the supernatant was measured by an ultraviolet spectrophotometer; the result is shown in Fig. S3. The concentration of Apt-luminol in the supernatant was calculated according to Lambert-Beer law, and the adsorption capacity of MCNTs to Apt-luminol was calculated to be 7.332×10^{-11} mol·mg^{-1}.

Optimization of method

The following parameters were optimized: (a) main pump speed; (b) vice pump speed; (c) concentration of NaOH; (d) concentration of H_2O_2. Respective text and Figures on optimizations are given in the Electronic Supplementary Material (Fig. S4). In short, the following experimental conditions were found to give best results: (a) optimal main pump speed: 45 r·min^{-1}; (b) optimal vice pump speed: 30 r·min^{-1}; (c) optimal NaOH concentration: 0.08 mol·L^{-1}; (d) optimal H_2O_2 concentration: 0.1 mol·L^{-1}.

The analytical performance of CL method

In order to prove that the presented CL method based on hemin@HKUST-1 catalysis can be used for detecting lysozyme, a calibration plot with the CL value and lysozyme concentration as variables was measured. Figure 2 illustrates that the CL value of the system increase with increasing lysozyme concentration, and the CL intensity is linearly related to the logarithm of lysozyme concentration ($c_{lysozyme}$) in the range from 1.05×10^{-6} U·mg^{-1} (6.0×10^{-13} mol·L^{-1}) to 1.25×10^{-2} U·mg^{-1} (7.14×10^{-9} mol·L^{-1}). The linear equation is $I = 557.28 \lg c + 10{,}845.75$ ($R^2 = 0.99$). The detection limit is 3.50×10^{-7} U·mg^{-1} (2.0×10^{-13} mol·L^{-1}). This is a good result for detecting lysozyme.

To demonstrate that the presented CL assay was meaningful for the detection of lysozyme, we compared the performance of the presented CL method with that of other excellent

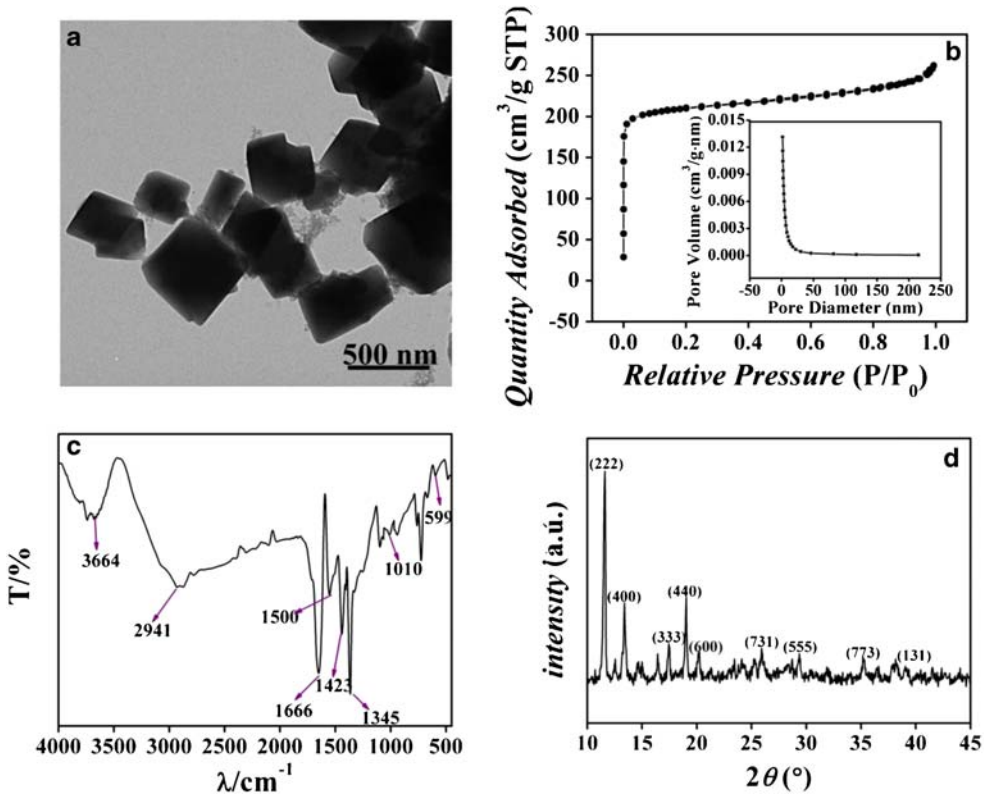

Fig. 1 TEM (**a**), BET (**b**), FTIR (**c**), and XRD (**d**) of hemin@HKUST-1

methods, as shown in Table 1. The results show that the present method possessed a lower detection limit and a wider linear range.

Reproducibility and stability of the CL assay

The reproducibility of the CL assay was investigated by measuring 11 identical samples. As shown in Fig. S5, the RSD of the presented CL assay is calculated to be 0.6%, indicating that the method has excellent precision.

When the experiment was completed, the reusability of the materials was explored. The collected wasted liquid was centrifuged, and the precipitate was dispersed in phosphate buffer. The mixture was heated to 95 °C. After 1 min, the solution was centrifuged, and the supernatant was collected. The precipitate was washed with phosphate buffer for several times, and the supernatant was collected every time. The CL intensity was measured when the concentration was 2.31×10^{-5} U·mg^{-1}. As shown in Fig. S6, after 7 cycles, the CL intensity of the method decreased from 10,531 to 10,319. There was 2.5% CL intensity loss in 10 days, indicating that materials possessed good reusability.

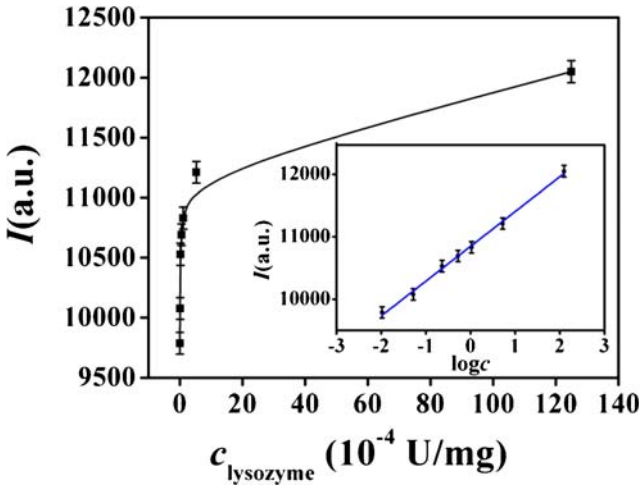

Fig. 2 The calibration plot of the CL assay ($n = 3$). Experimental conditions: chemiluminescence emission wavelength: 425 nm; photomultiplier tube high voltage: 600 V; number of signal amplification stages: 1

Table 1 Comparison results of different methods

Methods	Liner range (mol·L^{-1})	Detection limit (mol·L^{-1})
Colorimetry [27]	3×10^{-9}–1.5×10^{-7}	1.5×10^{-9}
Fluorescence [28]	2×10^{-8}–1.8×10^{-7}	2×10^{-8}
Electrochemiluminescence [29]	2.2×10^{-12}–5×10^{-8}	7.3×10^{-13}
Plasmon resonance light-scattering [30]	5×10^{-9}–1.6×10^{-6}	2.32×10^{-9}
Electrochemistry [31]	1×10^{-12}–1×10^{-8}	3.2×10^{-13}
This work	6×10^{-13}–7.14×10^{-9}	2×10^{-13}

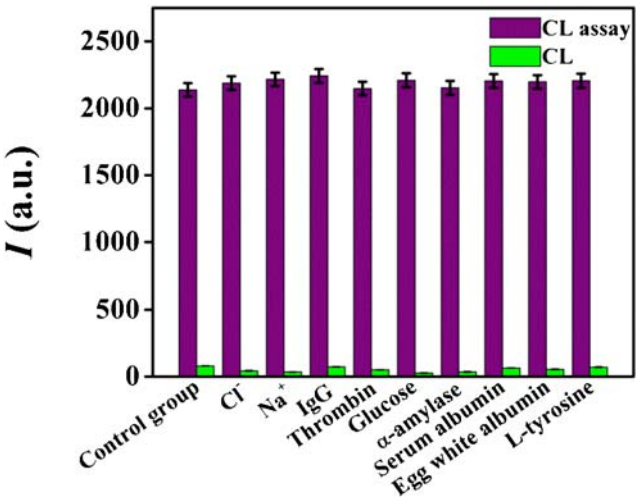

Fig. 3 The selectivity study of the CL assay. CL spectrum of the mixture containing coexistants were measured by a simple CL method and CL assay, respectively

For long-term stability evaluation, the materials were placed at 4 °C for 10 days, the CL intensity was measured (Fig. S7). After 10 days, the CL intensity of the method decreased from 12,058 to 11,762. There was 2.5% CL intensity loss in 10 days, suggesting workable application prospect.

Selectivity of the CL assay

To demonstrate that the CL assay was capable of detecting lysozyme in complex samples, the selectivity of the assay was explored. Cl^-, Na^+, HCO_3^-, IgG, thrombin, glucose, α-amylase, serum albumin, egg white albumin, and L-tyrosine were selected as coexistants and added to the lysozyme standard solution, respectively. The CL intensity of each solution was measured under optimal experimental conditions. While the tolerable limits of coexisting species were taken as a relative error no larger than 5%, the results are shown in Fig. 3. Due to the presence of hemin@HKUST-1, the CL intensity of CL assay is significantly higher than that of simple CL method. The CL assay possessed strong anti-interference ability under the condition that the relative error does not exceed 5%.

Application of the CL assay

The practicability of the CL assay has been explored. After the collected saliva samples were diluted with phosphate buffer, the lysozyme in saliva was detected by the CL assay. As shown in Table 2, the recovery is the range from 97.4 to 102.8%. The recovery of the reported methods was shown in Table S1. The results obtained by the presented CL assay are comparable with that of the literatures, indicating that the method also has good analytical performance.

Catalytic activity of hemin@HKUST-1

In this work, hemin@HKUST-1 was synthesized as a catalyst for the luminol-NaOH-H_2O_2 CL system. Hemin contains a large porphyrin ring, which results in poor water solubility. What's more, hemin is easy to form a dimer in aqueous solution, which greatly affects its catalytic activity. It was reported that HKUST-1 is more hydrophilic than other MOFs [28]. Therefore, coating hemin in HKUST-1 not only maintains the catalytic activity of hemin but also improves the hydrophilicity of hemin. In addition, Cu^{2+} in HKUST-1 can adsorb H_2O_2 by forming a Cu^{2+}-HOOH complex [29] so that the concentration of H_2O_2 around or inside HKUST-1 is higher than that in the solution. After H_2O_2 enters the interior of HKUST-1, it reacts with the unsaturated coordination binding sites and hemin in HKUST-1 to produce reactive oxygen free radicals. Luminol was immobilized on the surface of HKUST-1 by base pairing interaction between aptamer and cDNA so that it can react with reactive oxygen radicals that diffused from the pores of HKUST-1. To investigate the types of reactive oxygen species produced by the catalytic reaction, CL experiments were performed and the results are shown in Fig. 4.

The luminol-NaOH-H_2O_2 CL system was used as a blank. As can be seen from Fig. 4, the CL intensity of the system containing hemin@HKUST-1 (luminol-NaOH-H_2O_2-hemin@HKUST-1) is much higher than that of the blank, which indicates that hemin@HKUST-1 possesses a strong catalytic effect on the luminol-NaOH-H_2O_2 system. P-benzoquinone and thiourea was used as the trapping agent

Table 2 Application of CL assay

Samples	Add (10^{-3} U·mg^{-1})	Content (10^{-3} U·mg^{-1})	Found (10^{-2} U·mg^{-1})	RSD (%)	Recovery (%)
Saliva 1#	8.75	3.66	1.24	0.5	99.8
Saliva 2#	8.75	3.41	1.24	0.6	102.6
Saliva 3#	8.75	3.57	1.21	0.8	97.4
Saliva 4#	8.75	3.57	1.24	0.6	100.8
Saliva 5#	8.75	3.39	1.24	0.5	102.8
Saliva 6#	8.75	3.33	1.21	0.6	100.2

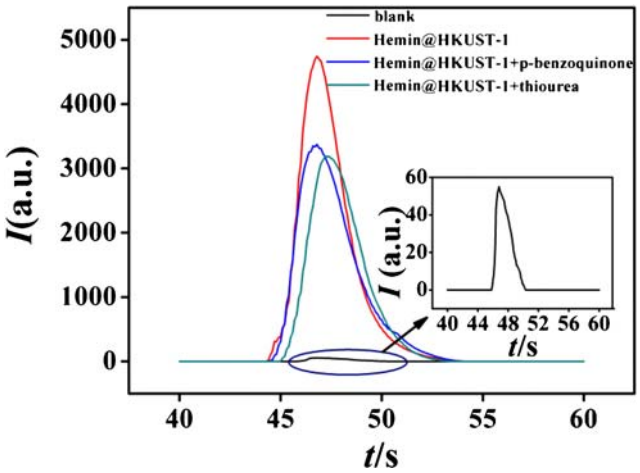

Fig. 4 Study on the types of active oxygen produced by hemin@HKUST-1. The CL spectrum of luminol-H_2O_2 system containing phosphate buffer, hemin@HKUST-1, hemin@HKUST-1–p-benzoquinone, hemin@HKUST-1–thiourea, respectively

of $\cdot O_2^-$ and ·OH, respectively. Then, the p-benzoquinone and thiourea were added to the luminol-NaOH-H_2O_2-hemin@HKUST-1 system, respectively. The CL intensity of luminol-NaOH-H_2O_2-hemin@HKUST-1-p-benzoquinone and luminol-NaOH-H_2O_2-hemin@HKUST-1-thiourea system is significantly lower than that of the luminol-NaOH-H_2O_2-hemin@HKUST-1 system. It is indicated that hemin and HKUST-1 can amplify CL signal of the system by catalyzing H_2O_2 to produce$\cdot O_2^-$ and ·OH.

Objective evaluation of the CL assay

It had been reported that under the condition of pH = 2, calcium alginate maintains a certain tensile strength and elasticity after being treated for 1 h. Singhal et al. [32] prepared a graphene oxide/calcium alginate composite for recovery of Au with a contact time of 22 h. At pH 1–5, the adsorption percentage of Au was very high, which indicates that the structure of calcium alginate was not destroyed completely. Treatment time of the present M-Alg-Apt with the eluent of pH = 2 was much less than 22 h. Therefore, the prepared M-Alg-Apt can maintain the structural integrity without affecting the signal amplification of the system.

The CL assay based on recycling amplification strategy was able to detect other targets by replacing different aptamers. However, this CL assay had the disadvantage that it cannot achieve on-line detection, which was also the goal we will strive to achieve in the future.

Conclusion

A CL assay was performed for the determination of lysozyme. Several advantages of the CL assay have been demonstrated: (1) M-Alg hydrogel was synthesized for the separation and enrichment of lysozyme from complex samples; (2) the complementary pairing between aptamer and cDNA shorten the distance from reactive oxygen radical to the luminol, and the CL efficiency was improved; (3) the target was circulated to release more signal tags, and the CL intensity was further enhanced to achieve sensitive determination of lysozyme. One major limitation of this method was that it can only achieve in vitro detection of the target and cannot achieve online real-time monitoring. The introduction of different aptamers enables determination of different targets, such as proteins, ions, and small molecules. Therefore, the method possesses potential for practical application.

Funding information This work was supported by the Shandong Provincial Natural Science Foundation of China (No. ZR2016BM01), Horizontal Scientific Research Project of China (No. W15077), National Natural Science Foundation of China (No. 21605094), The Youth Science fund of Shandong Academy of Sciences (No. 2017QN006), and Shandong Province Natural Science Institute Joint Fund (No. ZR2015YL006).

Compliance with ethical standards

Conflict of interest The authors declare that they have no competing interest.

References

1. Li FK, Gong AJ, Qiu LN, Zhang WW, Li JR, Liu Z (2019) Diglycolamide-grafted Fe_3O_4/polydopamine nanomaterial as a novel magnetic adsorbent for preconcentration of rare earth elements in water samples prior to inductively coupled plasma optical emission spectrometry determination. Chem Eng J 361:1098–1109
2. Wei J, Yang ZX, Sun Y, Wang CK, Fan JL, Kang GY, Zhang R, Dong XY, Li YF (2019) Nanocellulose-based magnetic hybrid aerogel for adsorption of heavy metal ions from water. J Mater Sci 54:6709–6718
3. Huang D, Wu JZ, Wang L, Liu XM, Meng J, Tang XJ, Tang CX, Xu JM (2019) Novel insight into adsorption and co-adsorption of heavy metal ions and an organic pollutant by magnetic graphene nanomaterials in water. Chem Eng J 358:1399–1409
4. Mortazavi-Derazkola S, Salavati-Niasari M, Khojasteh H, Amiri BO, Ghoreishi SM (2017) Green synthesis of magnetic Fe_3O_4/SiO_2/HAp nanocomposite for atenolol delivery and in vivo toxicity study. J Clean Prod 168:39–50
5. Alupei L, Peptu CA, Lungan AM, Desbrieres J, Chiscan O, Radji S, Popa M (2016) New hybrid magnetic nanoparticles based on chitosan-maltose derivative for antitumor drug delivery. Int J Biol Macromol 92:561–572
6. Wu K, Jing CY, Zhang J, Liu T, Yang SJ, Wang WD (2019) Magnetic Fe_3O_4@CuO nanocomposite assembled on graphene oxide sheets for the enhanced removal of arsenic(III/V) from water. Appl Surf Sci 466:746–756
7. Sun JH, Chen Y, Yu HQ, Yan LG, Du B, Pei ZG (2018) Removal of Cu^{2+}, Cd^{2+} and Pb^{2+} from aqueous solutions by magnetic alginate microsphere based on Fe_3O_4/MgAl-layered double hydroxide. J Colloid Interface Sci 532:474–484

8. Yu C, Sun H, Hou SF (2017) Direct electrochemistry and electrocatalysis of myoglobin immobilized in calcium alginate-graphene microspheres films. Anal Methods 9:4873–4881
9. Nirala NR, Pinker N, Desitti C, Shtenberg G (2019) Milk haptoglobin detection based on enhanced chemiluminescence of gold nanoparticles. Talanta 197:257–263
10. Bodulev OL, Gribas AV, Sakharov IY (2018) Microplate chemiluminescent assay for HBV DNA detection using 3-(10′-phenothiazinyl)propionic acid/N-morpholinopyridine pair as enhancer of HRP-catalyzed chemiluminescence. Anal Biochem 543: 33–36
11. Karan R, Capes MD, DasSarma S (2012) Function and biotechnology of extremophilic enzymes in low water activity. Aquat Biosyst 8:4–18
12. Meng R, Liu Q, Jin Y, Li BX (2018) Dual-hemin-labelled catalytic molecular beacon: a monomer-dimer switching probe for sensitive chemiluminescence detection of biomolecules. ChemistrySelect 3: 1908–1914
13. Zhou Z, Hartmann M (2013) Progress in enzyme immobilization in ordered mesoporous materials and related applications. Chem Soc Rev 42:3894–3912
14. Liu X, Qi W, Wang YF, Su RX, He ZM (2017) A facile enzyme immobilization strategy with high stable hierarchically porous metal-organic frameworks. Nanoscale 9:17561–17570
15. Alizadeh N, Salimi A, Hallaj R, Fathi F, Soleimani F (2018) Ni-hemin metal-organic framework with highly efficient peroxidase catalytic activity: toward colorimetric cancer cell detection and targeted therapeutics. J Nanobiotechnol 16:93–106
16. Luo FQ, Lin YL, Zheng LY, Lin XM, Chi YW (2015) Encapsulation of hemin in metal-organic frameworks for catalyzing the chemiluminescence reaction of the H_2O_2-luminol system and detecting glucose in the neutral condition. ACS Appl Mater Interfaces 7:11322–11329
17. Revenis ME, Kaliner MA (1992) Lactoferrin and lysozyme deficiency in airway secretions: association with the development of brochopulmonary dysplasia. J Pediatr 21:262–270
18. Tomita H, Sato S, Matsuda R, Sugiura Y, Kawaguchi H, Niimi T, Yoshida S, Morishita M (1999) Serum lysozyme levels and clinical features of sarcoidosis. Lung 177:161–167
19. Chen ZX, Xu Q, Tang GX, Liu S, Xu SX, Zhang XF (2019) A facile electrochemical aptasensor for lysozyme detection based on target-induced turn-off of photosensitization. Biosens Bioelectron 126:412–417
20. Dionisia O, Valle M (2018) Label-free aptasensor for lysozyme detection using electrochemical impedance spectroscopy. Sensors 18:354–364
21. Zhang ZH, Zhang S, He LH, Peng DL, Yan FF, Wang MH, Zhao JH, Zhang HZ, Fang SM (2015) Feasible electrochemical biosensor based on plasma polymerization-assisted composite of polyacrylic acid and hollow TiO_2 spheres for sensitively detecting lysozyme. Biosens Bioelectron 74:384–390
22. Dong YP, Wang J, Peng Y, Zhu JJ (2017) A novel aptasensor for lysozyme based on electrogenerated chemiluminescence resonance energy transfer between luminol and silicon quantum dots. Biosens Bioelectron 94:530–535
23. Ding WH, Guan LM, Han JJ, Mangala R, Luo ZX (2017) Fluorescence chemosensing of water-soluble Ag_{14} nanoclusters for lysozyme and Hg^{2+} ions. Sensors Actuators B Chem 250: 364–371
24. Li J, Mu XJ, Chan KC, Ko CC, Li MJ (2018) Sensitive determination of lysozyme by using a luminescent and colorimetric probe based on the aggregation of gold nanoparticles induced by an anionic ruthenate(II) complex. Microchim Acta 185:428–433
25. Guo YP, Zhou Y, Jia DC, Meng QC (2008) Fabrication and in vitro characterization of magnetic hydroxycarbonate apatite coatings with hierarchically porous structures. Acta Biomater 4:923–931
26. Chen J, Yu C, Zhao YL, Niu YZ, Zhang L, Yu YJ, Wu J, He JL (2017) A novel non-invasive detection method for the FGFR3 gene mutation in maternal plasma for a fetal achondroplasia diagnosis based on signal amplification by hemin-MOFs/PtNPs. Biosens Bioelectron 91:892–899
27. Shrivas K, Nirmalkar N, Deb MK, Dewangan K (2019) Jayant Nirmalkar, Suneel Kumar, Application of functionalized silver nanoparticles as a biochemical sensor for selective detection of lysozyme protein in milk sample Spectrochim Acta A Mol Biomol Spectrosc 213:127–133
28. Zeng Y, Zhang D, Qi P, Zheng LB (2018) Label-free simultaneous sensor for multi-components detection based on G-Quadruplex DNA structure. Sensors Actuators B Chem 265:468–475
29. Du FK, Zhang H, Tan XC, Yan J, Liu M, Chen X, Wu YY, Feng DF, Chen QY, Cen JM, Liu SG, Qiu YQ, Han HY (2018) $Ru(bpy)_3{}^{2+}$-silica@poly-L-lysine-Au as labels for electrochemiluminescence lysozyme aptasensor based on 3D graphene. Biosens Bioelectron 106:50–56
30. Fu F, Li LY, Luo QM, Li QJ, Guo TG, Yu MQ, Song Y, Song EQ (2018) Selective and sensitive detection of lysozyme based on plasmon resonance light-scattering of hydrolyzed peptidoglycan stabilized-gold nanoparticles. Analyst 143:1133–1140
31. Cao XY, Xu JY, Xia JF, Zhang FF, Wang ZH (2018) An electrochemical aptasensor based on the conversion of liquid-phase colorimetric assay into electrochemical analysis for sensitive detection of lysozyme. Sensors Actuators B Chem 255:2136–2142
32. Saha S, Venkatesh M, Basu H, Pimple MV, Singhal RK (2019) Recovery of gold using graphene oxide/calcium alginate hydrogel beads from a scrap solid state detector. J Environ Chem Eng 7: 103134–102140